Available online at www.sciencedirect.com
SCIENCE DIRECT®
International Journal of Heat and Mass Transfer 47 (2004) 1499–1513
International Journal of HEAT and MASS TRANSFER
www.elsevier.com/locate/ijhmt

Modelling of local two-phase flow parameters in upward subcooled flow boiling at low pressure

Boštjan Končar *, Ivo Kljenak, Borut Mavko

Jožef Stefan Institute, Jamova 39, SI-1000 Ljubljana, Slovenia

Abstract

The subject of the present work is a multidimensional modelling of vertical upward subcooled boiling flow using a two-fluid approach and calculation of local two-phase flow parameters (void fraction and bubble size). The dependence of bubble diameter on local flow conditions was taken into account. A sensitivity analysis of closure equations showed that besides phase-change mechanisms, the transverse hydrodynamic mechanisms also have to be considered for modelling of subcooled flow boiling at low-pressure conditions. The evolution of cross-sectional distributions of void fraction and local bubble diameter along the flow was simulated and compared to low-pressure experimental data from the literature [Experimental investigation of subcooled boiling, M.S.N.E. Thesis, Purdue University, West Lafayette, IN, USA, 1999; Int. J. Multiphase Flow 28 (2002) 1351].
© 2003 Elsevier Ltd. All rights reserved.

Keywords: Subcooled boiling flow; Void distribution; Two-fluid model; Multidimensional modelling

1. Introduction

Subcooled flow boiling denotes the process of evaporation of liquid flowing near a heated surface (usually channel wall), when the bulk flow temperature is lower than the local saturation temperature. The liquid temperature near the heated surface exceeds the saturation temperature and then gradually decreases (below saturation temperature) as the distance from the surface increases. Although subcooled boiling may appear in the form of different boiling regimes, the present work deals only with *nucleate* subcooled boiling, in which liquid evaporates in the form of vapour bubbles and a two-phase layer occurs near the heated surface. Among many industrial systems, subcooled flow boiling is important in water-cooled nuclear reactors, where the presence of vapour influences the system reactivity.

One may categorize subcooled boiling according to system pressure. The essential quantitative difference between boiling at so-called "high-pressure" and "low-pressure" conditions (below 10 bar) is the order of magnitude of the difference between liquid and vapour densities. At low pressure, nucleated bubbles are larger and move farther away from the heated wall into the cooler liquid before condensing, thus creating a different flow structure. The increased interest to investigate low-pressure subcooled boiling, which has appeared in recent years, is mainly due to the need to perform safety analyses of low-pressure research reactors and to investigate the sump-cooling concept for so-called advanced light water reactors.

In subcooled boiling flow in a vertical channel, not only is vapour unevenly distributed over the channel cross-section, but, in addition, the distribution evolves along the flow, as both the void fraction and the width of the two-phase layer near the heated surface gradually increase. This non-homogeneous distribution of vapour significantly influences hydrodynamic and thermal processes, including heat transfer. Although a considerable amount of literature deals with the cross-sectional distribution of the gas phase in adiabatic bubbly flow, investigations of analogous phenomena in boiling flow have been much less common.

Many experiments on subcooled boiling flow in channels have been performed over the past decades. As

* Corresponding author. Tel.: +386-1-588-5260; fax: +386-1-561-2335.
E-mail address: bostjan.koncar@ijs.si (B. Končar).

0017-9310/$ - see front matter © 2003 Elsevier Ltd. All rights reserved.
doi:10.1016/j.ijheatmasstransfer.2003.09.021

Nomenclature

A_{bub}	non-dimensional bubble influence area
A_i	interfacial area concentration (m^{-1})
A_w	heated area (m^2)
$A_{1\phi}$	non-dimensional single-phase convection area
Bo	boiling number $= q_w/Gh_{fg}$
C_L	lift force coefficient
C_{TD}	turbulent dispersion force coefficient
C_1, C_2	wall lubrication force coefficients
$C_{\mu b}$	coefficient in the Sato model of bubble induced turbulence
c_{pl}	liquid specific heat ($J\,kg^{-1}\,K^{-1}$)
c_w	specific heat of solid wall ($J\,kg^{-1}\,K^{-1}$)
D_h	channel hydraulic diameter (m)
d_b	bubble diameter (m)
d_{bw}	bubble departure diameter (m)
f	bubble nucleation frequency (s^{-1})
G	mass flow rate ($kg\,m^{-2}\,s^{-1}$)
h_{if}	interfacial heat transfer coefficient ($W\,m^{-2}\,K^{-1}$)
h_{fg}	latent heat ($J\,kg^{-1}$)
h_Q	quenching heat transfer coefficient ($W\,m^{-2}\,K^{-1}$)
$h_{1\phi}$	single-phase convection heat transfer coefficient ($W\,m^{-2}\,K^{-1}$)
k	turbulent kinetic energy of liquid ($m^2\,s^{-2}$)
k_l	liquid thermal conductivity ($W\,m^{-1}\,K^{-1}$)
k_w	thermal conductivity of solid wall ($W\,m^{-1}\,K^{-1}$)
N_a	number of active nucleation sites per unit area (m^{-2})
$\vec{n}$	unit normal vector
Nu_b	bubble Nusselt number
p	pressure (Pa, bar)
q_e	evaporation heat flux ($W\,m^{-2}$)
q_Q	quenching heat flux ($W\,m^{-2}$)
q_w	wall heat flux ($W\,m^{-2}$)
$q_{1\phi}$	single-phase convection heat flux ($W\,m^{-2}$)
r	radial coordinate
St	Stanton number $= Nu/RePr_l$
T	temperature (K)
v	velocity ($m\,s^{-1}$)
V	control volume (m^3)
y_w	distance from the near-wall computational cell (m)
y^+	non-dimensional distance
z	axial coordinate (m)

Greek symbols

α	void fraction
Γ	mass transfer rate ($kg\,s^{-1}\,m^{-3}$)
μ_l	molecular liquid viscosity ($N\,s\,m^{-2}$)
μ_l^{turb}	turbulent viscosity of liquid ($N\,s\,m^{-2}$)
μ_l^{eff}	effective viscosity of liquid ($N\,s\,m^{-2}$)
μ_l^b	bubble induced viscosity of liquid ($N\,s\,m^{-2}$)
ρ	density ($kg\,m^{-3}$)
ρ_w	density of solid wall ($kg\,m^{-3}$)
τ_G	bubble growth period (s)
τ_Q	quenching period (s)

Subscripts

g	vapour phase
in	inlet conditions
i	interface
l	liquid phase
sat	saturation
sub	subcooling
w	wall

Superscripts

d	drag related
l	lift force related
td	turbulent dispersion force related
w	wall related
wl	wall lubrication force related

the emphasis of the present work is on the multidimensional aspects of subcooled boiling, experiments in which the non-homogeneous cross-sectional distributions of flow parameters were not investigated, but only cross-sectional averages were determined (such as void fraction or heat transfer coefficient, related to the cross-sectional average temperature) are not considered here. Besides, our scope is limited to experiments in which water was used as a working fluid. Numerous experiments that were performed with refrigerants at low pressure are not considered, as they are supposed to simulate boiling of water at high-pressure conditions, which is not the subject of the present work.

Possibly the earliest experimental investigations of the multidimensional character of subcooled boiling were performed by St Pierre and Bankoff [3], who observed subcooled boiling in a vertical rectangular channel with heated walls at pressures ranging from 200 to 800 psia (1.4 to 5.5 bar). They have measured transverse void fractions over the channel cross-section at different elevations. Nylund et al. (1967, as cited by Anglart and Nylund [4]) have measured radial void fraction profiles in an annular test section with a heated inner rod at pressure 47 bar, and in a test section with six heated rods at pressure 49.7 bar. Later, Sekoguchi et al. [5] have determined radial void fraction profiles in cylindrical

tubes with heated walls at pressures 2, 4 and 8 atm. Much recently, Bartel [1] has obtained radial profiles of flow parameters at different axial locations in a vertical annulus with a heated inner rod, at near atmospheric pressure. Lee et al. [2] have also performed similar experiments at comparable flow conditions, but have reported radial distributions of flow parameters only at a single axial location.

Among multidimensional theoretical descriptions of subcooled boiling, the most widely used approach so far appears to be two-fluid modelling. Thus, Kurul and Podowski [6], Lai and Farouk [7], Anglart and Nylund [4], Lahey Jr. and Drew [8], and Roy et al. [9] have all proposed their own modifications of the two-fluid model. However, their models have been applied either to boiling of water at high pressure or to boiling of refrigerants at low pressure. Unfortunately, the extrapolation of models developed for water at high-pressure conditions to low pressure usually leads to erroneous results. Extrapolations of models developed for high-pressure conditions to low pressure have so far been attempted only for one-dimensional two-fluid models [10,11]. Namely, although the generic features of the two-fluid model are the same, many closure relations describing mass, momentum and energy exchange at the gas–liquid interface do not apply to both high-pressure and low-pressure conditions.

Multidimensional two-fluid models of subcooled boiling flow of water at low pressure have been proposed by Janssens-Maenhout et al. [12], Tu and Yeoh [13] and Lee et al. [2]. All of them applied the general-purpose computational fluid dynamics (CFD) code CFX. Lee et al. [2] have successfully applied their model to the simulation of their own experimental results, whereas Tu and Yeoh [13] and Janssens-Maenhout et al. [12] have presented only evolutions of cross-sectional average quantities along the flow.

Some promising approaches for modelling of boiling based on local instantaneous description of the flow field have also been proposed [14,15]. However, due to the complex structure of the interface in subcooled nucleate boiling, these approaches are still computationally too demanding for simulating boiling systems over a significant portion of a channel. Another approach which is worth mentioning is the so-called bubble-tracking modelling, in which vapour bubbles are considered individually [16,17].

In the present work, a two-fluid model of upward subcooled nucleate boiling flow in a vertical channel at low-pressure conditions is proposed. The model consists of a generic two-fluid model, which is implemented within the CFX code, and additional closure relations introduced by the authors. The model was validated by comparing calculated results to experimental data from other authors [1,2]. To the best of the authors' knowledge, this is the first attempt to simulate the evolution of cross-sectional distributions of two-phase flow parameters along the flow at low-pressure conditions using a two-fluid model.

2. Two-fluid model of subcooled nucleate flow boiling

The two-fluid model of subcooled nucleate boiling flow consists of a dispersed phase (vapour bubbles) and a continuous phase (liquid flow) and is based on two sets of averaged transport equations. At averaging, the so-called "interpenetrating continua" approach is used, where each phase is treated as a continuum that fills up the entire control volume and is described by its own system of averaged equations for mass, momentum and energy. Averaged equations for both phases are coupled with additional closure relations describing the exchange of mass, momentum and energy at the interface as well as the turbulence within each phase. The two-fluid model has been described extensively in many works [18,19].

In the present work, the general-purpose computational fluid dynamics (CFD) code CFX-4.3 [20] was used as a framework for solving the generic two-fluid model with additional relevant closure relations, introduced by the authors, which describe the mechanisms of phase change and lateral transport of mass, momentum and energy. The discretisation of transport equations in the CFX-4.3 code is based on a conservative finite-volume method. A non-staggered grid arrangement is employed, where all variables (velocity components and scalars) are stored in the geometrical centres of control volumes (cells) that fill up the considered flow domain.

The emphasis of the present paper is on the description of the closure relations and the analysis of calculated results.

2.1. Turbulence modelling

Due to the lower density of vapour, it is commonly assumed that, in nucleate boiling flow, the motion of the dispersed vapour phase follows the fluctuations in the continuous liquid phase [6]. Accordingly, the turbulence stresses are modelled only for the liquid phase, whereas the vapour phase is assumed to be laminar. In the present work, the following option from the CFX-4.3 code was applied: turbulence in the liquid phase is modelled using a k–ε model with an additional term describing the bubble-induced turbulence. Shear and bubble-induced turbulence are linearly superimposed, according to an assumption from Sato et al. [21], where the effective viscosity of the continuous liquid phase is expressed as:

$$\mu_{\mathrm{l}}^{\mathrm{eff}} = \mu_{\mathrm{l}} + \mu_{\mathrm{l}}^{\mathrm{turb}} + \mu_{\mathrm{l}}^{\mathrm{b}}. \quad (1)$$

The bubble-induced turbulence viscosity μ_l^b in the liquid phase depends on the vapour phase volume fraction α, the local bubble diameter d_b and the relative velocity between the phases:

$$\mu_l^b = C_{\mu b}\rho_l \alpha d_b |\vec{v}_g - \vec{v}_l|. \quad (2)$$

In the present work, the coefficient $C_{\mu b}$ was set to the value 0.6, as recommended by Sato et al. [21]. The liquid phase turbulence in the near wall region is described by so-called "wall functions". The turbulent boundary layer near the wall consists of a very thin laminar sublayer adjacent to the wall and a so-called "buffer region", which describes the flow between the laminar sublayer and the core of the turbulent flow (modelled with the k–ε model). The thickness of the laminar sublayer is defined by the non-dimensional distance from the wall $y^+ = 11.23$ [22]. In the laminar sublayer, the axial liquid velocity is a linear function of the distance from the wall. In the buffer region ($11.23 \leqslant y^+ \leqslant 300$), the velocity profile is described by the logarithmic wall function [22].

2.2. Interphase momentum transfer

In the CFX-4.3 code, the interphase transfer of momentum in bubbly flows is modelled with the following interfacial forces: drag force, lift force, turbulent dispersion force and wall lubrication force [20]. The interphase drag force is flow-regime dependent and is modelled according to a correlation by Ishii and Zuber [23]. The lift force on the liquid phase can be calculated as [20]:

$$\vec{F}_L = \alpha C_L \rho_l (\vec{u}_g - \vec{u}_l) \times \nabla \times (\vec{u}_l), \quad (3)$$

where C_L is the lift force coefficient and was set to the value 0.1, which is adequate for weakly turbulent bubbly flow [24]. This force is shear-induced and pushes the bubbles towards the wall (i.e. towards the lower velocity region). The effect of diffusion of the vapour phase, caused by liquid phase turbulence, is described with the turbulent dispersion force:

$$\vec{F}_{TD} = -C_{TD}\rho_l k \nabla \alpha, \quad (4)$$

where k is the turbulent kinetic energy of the liquid phase and C_{TD} is the turbulent dispersion coefficient, which was set to 0.1 according to Kurul and Podowski [6]. Since the drainage rate of liquid is restrained by the no-slip condition at the wall, the wall lubrication force acts in the radial direction away from the wall and prevents the accumulation of bubbles near the wall. The wall lubrication force is modelled using a correlation from Antal et al. [25]:

$$\vec{F}_W = \frac{\alpha\rho_l(\vec{u}_g - \vec{u}_l)^2}{d_b} \cdot \max\left(C_1 + C_2\frac{d_b}{y_w}, 0\right)\vec{n}, \quad (5)$$

where y_w denotes the distance from the wall. According to Eq. (5), the wall lubrication force strongly depends on the local bubble diameter d_b. In the present work, the coefficient values were set as $C_1 = -0.04$ and $C_2 = 0.08$ to obtain a good agreement between calculated and experimental void fraction radial profiles. With this set of coefficients, the wall lubrication force acts within the region of two bubble diameters away from the heated wall.

2.3. Interfacial condensation

In various subcooled boiling experiments, different behaviour of bubbles near the heated surface has been observed. At low-pressure conditions, a majority of investigators [26–28] agree on the following physical picture: bubbles generated at the heated wall slide along the wall, eventually depart and travel further with the subcooled flow, where they are subject to condensation.

In the present model of subcooled flow boiling, heat and mass exchange between the phases are described by bubble evaporation on the heated wall (Section 2.4) and by bubble condensation in the subcooled liquid flow. After departure from the heated wall, a bubble is supposed to be surrounded by the subcooled liquid. When the liquid surrounding a bubble is subcooled, the vapour inside the bubble and the bubble interface are assumed to be at saturation temperature. The interfacial condensation rate Γ_{cond} across the phase boundary is calculated as:

$$\Gamma_{cond} = \frac{h_{if}A_i(T_{sat} - T_l)}{h_{fg}}, \quad (6)$$

where A_i is the interfacial area per unit volume, h_{fg} is the latent heat and h_{if} is the interphase heat transfer coefficient, defined by the bubble Nusselt number Nu_b:

$$h_{if} = \frac{Nu_b k_l}{d_b}, \quad (7)$$

where Nu_b is calculated from the Ranz-Marshall correlation (from [20]). The bubbles in the proposed two-fluid model are assumed to have a spherical shape, so that the interfacial area A_{if} is expressed as $6\alpha/d_b$, α being the vapour volume fraction.

2.4. Wall evaporation model

Modelling of the heat transfer term at the wall is one of the most important issues in simulation of flow boiling. The mechanisms controlling the heat transfer from the wall to each phase are complex and although nucleate flow boiling has been intensively investigated in

the past {Bowring (1962, as cited by Bibeau and Salcudean [26]), Meister [29], Victor et al. [30]}, a lot of research effort is still needed to satisfactory understand the process.

In the present work, the model of Kurul and Podowski [6], which is basically included in the CFX-4.3 code, is used. According to this model, each unit of the heated surface is split into two parts: one part of the heated area is influenced by the nucleating bubbles A_{bub}, whereas the other part $A_{1\phi}$ is influenced only by the single-phase convection. In non-dimensional form, A_{bub} and $A_{1\phi}$ represent the fractions of the total heated area:

$$A_{\text{bub}} + A_{1\phi} = 1. \tag{8}$$

The heat flux from the wall to the nucleate boiling flow consists of three different components:

$$q_{\text{w}} = q_{1\phi} + q_{\text{Q}} + q_{\text{e}}, \tag{9}$$

where

- $q_{1\phi}$ denotes the single-phase convection heat flux that takes place outside the influence area of the nucleating bubbles,
- q_{Q} denotes the heat flux, within the bubble influence area, from the wall to the fresh bulk liquid that periodically fills the volume vacated by departing or collapsing bubbles during the bubble ebullition cycle (so-called "quenching heat flux"),
- q_{e} denotes the wall evaporation heat flux, that is needed for direct generation of vapour bubbles.

The bubble influence area per unit wall area A_{bub} is determined as:

$$A_{\text{bub}} = \min\left[1, N_{\text{a}} K \left(\frac{\pi d_{\text{bw}}^2}{4}\right)\right], \tag{10}$$

where N_{a} is the number of active nucleation sites per unit wall area and d_{bw} is the maximum bubble diameter at departure. The parameter K determines the size of the bubble influence area around the nucleation site on the heated wall that is subject to the quenching heat transfer. Mostly, the constant value of $K = 4$ is recommended [30]. Assuming that $K = 4$ and that the overlapping between two neighbouring and simultaneously nucleating bubbles is neglected, the minimum spacing between two neighbouring nucleation sites is 2 bubble diameters d_{bw}. Thus, at maximum density of nucleation sites N_{a}, the bubble influence area is equal to the total heating surface ($A_{\text{bub}} = 1$).

The single-phase convection heat flux outside the bubble influence area is calculated as:

$$q_{1\phi} = h_{1\phi} \cdot A_{1\phi} \cdot (T_{\text{w}} - T_{\text{l}}), \tag{11}$$

where $h_{1\phi}$ is the single-phase liquid heat transfer coefficient, T_{w} is the wall temperature and T_{l} is the local liquid temperature in the near-wall computational cell. The coefficient $h_{1\phi}$ for turbulent convective flow is determined via the local Stanton number as:

$$h_{1\phi} = St \cdot \rho_{\text{l}} \cdot c_{\text{pl}} \cdot v_{\text{l}}, \tag{12}$$

where the local Stanton number St is calculated according to Kurul [31].

The quenching heat flux is modelled as a transient conduction from the wall to a semi-infinite liquid at local temperature T_{l}:

$$q_{\text{Q}} = h_{\text{Q}} A_{\text{bub}} (T_{\text{w}} - T_{\text{l}}), \tag{13}$$

where h_{Q} is the quenching heat transfer coefficient according to Victor et al. [30]:

$$h_{\text{Q}} = \left(\frac{2 \cdot \sqrt{k_{\text{l}} \rho_{\text{l}} c_{\text{pl}}}}{\sqrt{\pi \tau_{\text{Q}}}}\right) f \cdot \tau_{\text{Q}}. \tag{14}$$

The quenching period τ_{Q} between the departure of a bubble and the beginning of the growth of a subsequent one is defined as [6]:

$$\tau_{\text{Q}} = 0.8 \frac{1}{f}. \tag{15}$$

Ivey [32] noted, that the portion of the quenching period τ_{Q} in the total time interval $1/f$ might vary with the heat flux. For low and medium heat fluxes, this portion assumes values between 0.5 and 1. In the proposed model (Eq. (15)), it is assumed that 80% of the total time interval between successive bubble nucleations is used for the heating of the bulk liquid by the quenching heat flux. According to Eqs. (13) and (14), a decreased quenching period reduces the quenching heat flux q_{Q}. Since the bubble is longer in contact with the heated wall (for instance, if the bubble slides along the heated surface), more time is allowed for evaporation, which causes the increase of evaporation heat flux q_{e}.

In the present work, additional bubble evaporation during sliding (at low pressure, bubbles slide immediately after boiling incipience until departure from the wall) has been taken into account implicitly in the model of bubble departure diameter d_{bw} (Section 2.5). The evaporation heat flux q_{e} is proportional to the energy required for nucleation of a single bubble, the number of active nucleation sites per unit wall area N_{a} and the bubble nucleation frequency f:

$$q_{\text{e}} = N_{\text{a}} f \left(\frac{\pi}{6} d_{\text{bw}}^3\right) \rho_{\text{g}} h_{\text{fg}}. \tag{16}$$

The correlation of Lemmert and Chawla [33] was adopted to calculate N_{a}:

$$N_{\text{a}} = (m(T_{\text{w}} - T_{\text{l}}))^n. \tag{17}$$

Following Kurul and Podowski [6], the constants m and n are set to the values of 185 and 1.805, respectively. For

the bubble nucleation frequency, the relationship of Cole (1960, cited by Ivey [32]), was used:

$$f = \sqrt{\frac{4}{3}\frac{g(\rho_l - \rho_g)}{d_{bw}\rho_l}}, \tag{18}$$

where f is affected only by the bubble departure diameter d_{bw} and by phase densities ρ_l and ρ_g. Thus, the modelling of wall heat transfer in subcooled nucleate boiling largely depends on determining d_{bw}.

The remaining unknown in equations for heat flux components (11), (13), (16) is the wall temperature T_w, that can be calculated from the wall heat flux balance (Eq. (9)) with an iterative procedure using a bisection algorithm [20]. The wall temperature depends on the liquid temperature and velocities in the near-wall cell. This heat flux partitioning algorithm is used as a default algorithm in the CFX-4.3 code and presents a strongly coupled problem for the code solver.

When the heat flux components are calculated, the evaporation rate at the wall per unit volume Γ_w can be obtained from the evaporation heat flux q_e:

$$\Gamma_w = \frac{q_e}{(h_{fg} + c_{pl}\Delta T_{sub})}\frac{A_{w,i}}{V_i}, \tag{19}$$

where h_{fg} is the latent heat used to evaporate the liquid at saturation temperature, whereas $A_{w,i}$ and V_i are the heated area and volume of the ith near-wall cell. The second term in the denominator of Eq. (19) is used for heating of the subcooled liquid to the saturation temperature. It is assumed that the vapour inside the bubbles is at saturation condition.

2.5. Bubble departure diameter at the wall

According to many experimental results, the bubble departure diameter d_{bw} varies along the heated wall. The experimental data of Unal [34], Zeitoun and Shoukri [27], Bartel [1] and Prodanovic et al. [28] showed that at low pressure (of about 1 bar), bubble sizes significantly increased with decreasing subcooling along heated channels. The generated bubbles of spherical or ellipsoidal shape were relatively large (they reach maximum diameters of a few millimetres). In the original CFX-4.3 code, d_{bw} is modelled as a function of liquid subcooling.

In the present work, the authors applied Unal's [34] mechanistic model to describe the variation of bubble departure size along the heated wall. Unal assumed that a bubble is subject to simultaneous microlayer evaporation at the bottom and to condensation at the top. The bubble may slide or collapse on the heated surface during its lifetime. After reaching the maximum size, the bubble departs from the wall and migrates into the subcooled liquid, where it eventually collapses. Unal's mechanistic model describes the maximum bubble departure diameter d_{bw} as a function of pressure, liquid subcooling, heat flux and liquid flow velocity:

$$d_{bw} = C_{bw}\frac{2.42\times10^{-5}\cdot p^{0.709}a}{\sqrt{b\phi}}, \tag{20}$$

where coefficients a, C, b and ϕ are defined as:

$$a = \frac{(q_w - h_{1\phi}\cdot\Delta T_{sub})^{1/3}k_l}{2C^{1/3}h_{fg}\rho_g\sqrt{\pi k_l/\rho_l c_{pl}}}\sqrt{\frac{k_w\rho_w c_w}{k_l\rho_l c_{pl}}},$$

$$C = \frac{h_{fg}\mu_l\left[c_{pl}/(0.013h_{fg}Pr_l^{1.7})\right]^3}{\sqrt{\sigma/(\rho_l-\rho_g)g}},$$

$$b = \frac{\Delta T_{sub}}{2(1-\rho_g/\rho_l)},$$

$$\phi = \begin{cases} \left(\frac{v_l}{0.61}\right)^{0.47} & \text{for } v_l \geqslant 0.61\ \text{m s}^{-1}, \\ 1 & \text{for } v_l < 0.61\ \text{m s}^{-1}. \end{cases}$$

The range of applicability of the correlation is:

pressure: $0.1 < p < 17.7$ MPa,
wall heat flux: $0.47 < q_w < 10.64$ MW m^{-2},
liquid velocity: $0.08 < u_l < 9.15$ m s^{-1},
liquid subcooling: $3.0 < \Delta T_{sub} < 86$ K.

Since the heat flux in the considered experimental data is below the range of applicability of the correlation, the coefficient C_{bw} was added in Eq. (20) to describe relatively large bubbles at low-pressure conditions. The default value of C_{bw} is 2. However, this value had to be adjusted in some experimental cases (see Section 3).

2.6. Modelling of local bubble diameter in the flow domain

Bubble size determines the interfacial momentum transfer (drag force, wall lubrication force) as well as interfacial heat and mass transfer (evaporation and condensation). Since the maximum liquid temperature occurs at the heated wall, one could expect that the maximum value of local bubble diameter d_b would also occur there. However, the experimental data of Bartel [1] (see also Fig. 7) indicate that the maximum value of measured local bubble Sauter diameter is somewhat shifted away from the heated wall. The measured local bubble diameter first increases in the radial direction and then starts decreasing after reaching its maximum somewhere in the subcooled flow region.

Due to lack of experimental data about the size of bubble diameter or interfacial area concentration in subcooled flow boiling, many investigators assumed constant values of bubble diameter in the flow field and spherical shape of the bubbles to determine the interfacial area concentration A_i. Chatoorgoon et al. [35] used a bubble diameter of 2.5 mm in their one-dimensional subcooled boiling model. Lai and Farouk [7] prescribed a 1 mm bubble diameter in the flow field to perform two-dimensional numerical simulations of subcooled flow

boiling. Kurul and Podowski [6] and Anglart and Nylund [4] modelled the bubble diameter as a linear function of local liquid subcooling with maximum value of d_b located in the near-wall cell:

$$d_b = \frac{d_{b1} - d_{b0}}{\Delta T_{sub,1} - \Delta T_{sub,0}} \Delta T_{sub} + \frac{d_{b0}\Delta T_{sub,1} - d_{b1}\Delta T_{sub,0}}{\Delta T_{sub,1} - \Delta T_{sub,0}}. \quad (21)$$

This approach requires the prescription of minimum d_{b0} and maximum bubble diameter d_{b1}, at reference subcoolings, $\Delta T_{sub,0}$ and $\Delta T_{sub,1}$, respectively. To develop an adequate model of bubble diameter, it is necessary to understand the physical mechanisms, which control the bubble increase in the wall region. The possible reasons that may cause the increase of bubble diameter in the wall region are the following:

- Bubbles may coalesce before or after departure from the heated surface. However, bubble coalescence is probably not significant for the case of experiments simulated in the present work [1,2], since the local void fraction is always below 0.3.
- Very likely, a spectrum of bubble sizes (with mean bubble departure diameter d_{bw}) is being generated in every local region of the heated wall; in a given velocity and temperature field of liquid, larger bubbles migrate farther into the subcooled flow than smaller bubbles. Thus, the radial profile of measured local bubble diameter averaged over the spectrum of bubble sizes may increase with the distance from the wall until the condensation effect prevails.

In the original CFX-4.3 code, the local bubble diameter is treated as an adjustable parameter that is independent from the bubble departure diameter. In the present work, a simple model of radial distribution of bubble diameter is proposed. The shift of the maximum local bubble diameter away from the heated wall is modelled by a linear evolution in the radial direction as:

$$d_b^* = \min(d_{bw} + y_w, d_{b,max}), \quad (22)$$

where the bubble departure diameter d_{bw} is imposed in the near-wall cell. The radial distance from the near-wall cell center is denoted as y_w. The maximum allowed bubble diameter $d_{b,max}$ in the subcooled flow is prescribed as $2d_{bw}$. Eq. (22) is then multiplied by a relation describing the decrease of the bubble diameter due to condensation in the subcooled flow field:

$$d_b = d_b^* \cdot \exp\left(-\frac{\Delta T_{sub} - \Delta T_{sub,w}}{2 \cdot \Delta T_{sub,w}} \right) \quad (23)$$

where $\Delta T_{sub,w}$ is the local subcooling in the near-wall cell. Thus, in the proposed model, the local bubble diameter d_b in the flow field is coupled with the bubble departure diameter d_{bw} generated in the near-wall cell.

2.7. Saturation temperature

In the original CFX-4.3 code, the saturation temperature may be defined only as a constant value over the entire flow domain. In the present work, the saturation temperature is modelled as a function of local static pressure (according to steam tables). This is particularly important at near-atmospheric pressure, where the saturation temperature may vary substantially along the flow (for about 5 K in a 2 m long vertical tube) due to high relative pressure drop.

3. Results and discussion

The proposed two-fluid model of subcooled flow boiling was validated against two sets of low-pressure experimental data from the literature, Bartel [1] and Lee et al. [2]. In Bartel's [1] experiments, radial profiles of local void fraction and local bubble Sauter diameter were measured. As bubbles in the proposed model are assumed to be spherical, their diameters are equal to Sauter diameters and may therefore be compared to experimental results. In the work of Lee et al. [2], only radial profiles of void fraction at a single axial location are reported.

The subcooled flow boiling experiments of Bartel [1] were performed at atmospheric pressure. The experiments were carried out in a vertical annulus with a heated inner rod. The annular test section has inner and outer diameters of 19.1 and 38.1 mm, respectively. The length of the heated part of the annulus is 1.5 m, while the inlet part of the test section (0.635 m) is not heated. Electrical conductivity probes were used to measure local two-phase flow parameters, including void fraction, interfacial area concentration and bubble Sauter diameter. The data were collected at three different axial locations in the heated part of the test section with a fixed heater rod. Thus, the axial evolution of radial distributions of flow parameters was observed.

It should be noted that in the case of Bartel's experiments, the absolute pressure was not measured in any location of the experimental facility. Therefore, the pressure at the inlet of the heated section was estimated by the sum of the atmospheric pressure and the pressure difference due to the elevation between the test section inlet and the top of the separator tank, which was exposed to the atmosphere. A detailed geometrical description of the experimental facility is provided in the original reference [1]. Experiments were carried out at different values of mass flow rate, heat flux and inlet temperature. Experimental conditions are presented in Table 1.

Table 1
Experimental conditions of Bartel [1]

Experiment No.	q_w (kW m^{-2})	G (kg m^{-2} s^{-1})	v_{inlet} (m s^{-1})	T_{in} (K)
1	105	470	0.49	363.8
2	147	922	0.96	369.2
3	128	701	0.73	366.6
4	128	701	0.73	367.9
5	145	700	0.73	367.5

The second set of experimental data used in the present work was obtained by Lee et al. [2]. They have used a test channel of similar geometry and dimensions as the one used by Bartel [1]. The vertical annular test channel is 2.376 m long with a heated inner tube. The 1.67 m long inner tube with outer diameter of 19 mm is composed of a heated section with copper electrodes at both ends of the heated section. The outer tube consists of two stainless steel tubes of 37.5 mm inner diameter, which are connected below the measuring plane by a transparent 50 mm long glass tube.

Local measurements over the channel cross-section were performed only at one axial location, 1.61 m downstream of the beginning of the heated section. The temperature and absolute pressure were measured at the inlet. The measurement errors of mass flow rate, inlet subcooling and heat flux were estimated to be within ±1.8%, ±2.5% and ±1.7% of the related values, respectively. The system pressure was maintained between 1 and 2 bar. Local measurements of void fraction and vapour velocity were carried out using electrical conductivity probes. In the present work, four representative experimental cases, presented in Table 2, were simulated.

3.1. Numerical model of selected experiments

The flow through the annular vertical tube is assumed to be axis-symmetric. Therefore, the calculations were carried out on a two-dimensional computational domain in cylindrical r–z coordinates (Fig. 1).

Due to similar geometry and dimensions, both simulation domains (for Bartel's and Lee et al. test section) were divided into 20 radial and 200 axial cells. The unheated inlet sections were included in the domains, because the radial profiles of velocity and temperature at the inlet of the heated sections are not reported. Thus, in the simulations, profiles developed until the beginning of the heated section. Bartel's test section is represented by a 500 mm long unheated inlet part, followed by a 1500 mm long heated part. The inner and outer radii of the simulation domain are 9.55 and 19.05 mm, respectively. The test section of Lee et al. is represented by a 330 mm long unheated inlet part, followed by a 1670 mm long heated part. The inner and outer radii of Lee et al. computational domain are 9.5 and 18.75 mm, respectively.

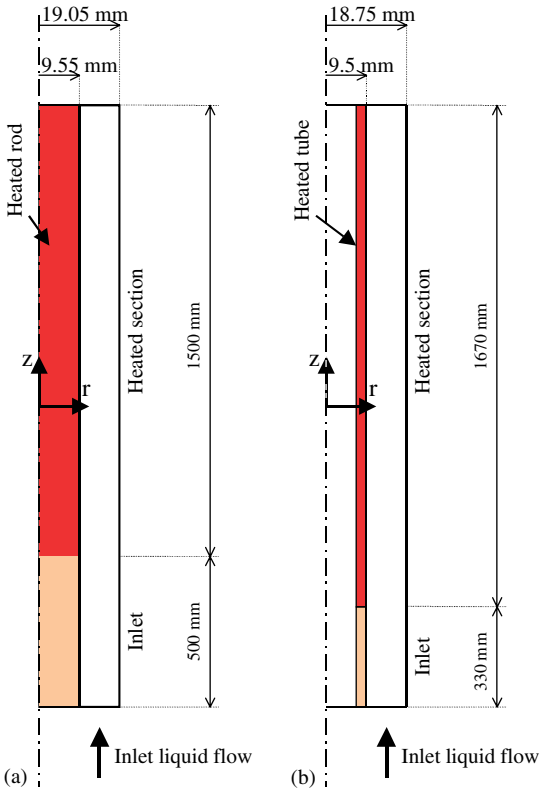

Fig. 1. Simulation domains of Bartel's (a) and Lee et al. (b) test section.

To solve the system of transport equations and closure relations, the appropriate boundary conditions were set. A free slip boundary condition for the vapour phase is used at the walls, taking into account the sliding

Table 2
Experimental conditions of Lee et al. [2]

Experiment No.	P_{inlet} (MPa)	q_w (kW m^{-2})	G (kg m^{-2} s^{-1})	T_{in} (°C)	$T_{sub(in)}$ (°C)
1	0.115	169.76	478.14	83.9	19.6
2	0.121	232.59	718.16	84	21.2
3	0.130	114.78	476.96	95.6	11.5
4	0.125	139.08	715.17	93.9	12.0

of the bubbles in the laminar sublayer. As a logarithmic wall function is used as a wall boundary condition for the liquid phase velocity, the dimension of the near-wall computational cell must satisfy the condition $y^+ > 11.23$. This requirement does not allow performing a systematic convergence analysis on different grids (which was also not reported in the works of other authors [9,13]). The location of the centre of the first computational cell is set to 0.5 mm away from the heated wall in both computational grids, so that y^+ assumes values between 50 and 80. A constant heat flux boundary condition is applied at the inner wall of the annulus. The outer wall of the annulus is assumed to be adiabatic. At the inlet, uniform velocity and temperature profiles are set according to Tables 1 and 2. At the outlet of the annulus, a pressure boundary condition is applied. The solution was considered to converge when relative errors of enthalpy flows (relatively to the added heat) were lower than 3% [36].

3.2. Sensitivity analyses of closure models

A series of parametric tests was performed to evaluate the effect of the most important closure relations on the radial distribution of local flow parameters. The tests were carried out on Bartel's case 4. This case was selected as illustrative, because neither the mass flux nor the wall heat flux assume extreme values in the considered ranges (see Tables 1 and 2).

3.2.1. Influence of bubble-induced turbulence

The influence of the bubble-induced turbulence model (Eqs. (1) and (2)) is shown on Fig. 2. Two calculations were performed, with different values of the coefficient $C_{\mu b}$ (0.6 and 0.01) in the model of Sato et al. (Eq. (2)). All other closure relations were kept unchanged. In the case of a low value of $C_{\mu b}$ (0.01), the effect of shear-induced turbulence prevails over the effect of bubble-induced turbulence. Fig. 2a shows the radial distribution of the effective viscosity of the liquid, where higher liquid viscosity means more intense turbulent mixing. In the case of prevailing shear-induced turbulence ($C_{\mu b} = 0.01$), the liquid viscosity is the highest in the central region of the annular gap, while it is lower near both walls. In the case of significant bubble-induced turbulence ($C_{\mu b} = 0.6$), the turbulent mixing of the liquid is most intense near the heated wall, where the bubbles are generated. Bubble-induced turbulence significantly enhances the transverse transport of mass, momentum and heat in the wall region, causing a flattening of the variable gradients (e.g. liquid temperature and axial liquid velocity, as shown in Fig. 2b and c). Due to the bubble-induced turbulence, the reduced temperature near the heated wall also influences the wall evaporation rate. As a lower temperature directly affects the calculation of the bubble departure diameter d_{bw} (Eq. (20)), a lower diameter d_{bw} is calculated along the heated wall for the simulation with $C_{\mu b} = 0.6$ (Fig. 2). Following Eq. (16), the lower value of diameter d_{bw} implies a lower evaporation heat flux q_e (Fig. 2e). Consequently, a lower wall evaporation rate results in a lower void fraction in the near-wall region (Fig. 2f). Thus, bubble-induced turbulence causes a lower void fraction in the near-wall region.

3.2.2. Influence of non-drag forces

The effect of the non-drag forces (turbulent dispersion: TD, lift force: LF and wall lubrication: WL) for Bartel's experimental case 4 is presented on Fig. 3. Four different calculations were performed to evaluate the effect of each non-drag force on the flow parameters. The forces were gradually added to the generic two-fluid model, whereas the other closures remained unchanged. Thus, the curve "None" indicates the calculation, where none of the non-drag forces is included in the two-fluid model, whereas the curve "TD + LF + WL" represents the calculation with all non-drag forces implemented in the model.

As shown on Fig. 3a, the inclusion of the turbulent dispersion force (TD) acts to flatten the radial void fraction profile. Similarly, the gradient of the liquid temperature (Fig. 3b) also decreases. As shown in Fig. 3a and b, the lift force has no significant effect on the lateral distribution of flow parameters. The additional inclusion of the wall lubrication force (TD + LF + WL) significantly improves agreement with experimental data. The wall lubrication force acts to push the vapour bubbles away from the wall and successfully reproduces the maximum void fraction located somewhat apart from the wall. However, the influence of the wall lubrication force on the liquid temperature is not significant. Finally, one can see that the calculation without non-drag forces (None) gives the poorest prediction of local void fraction distribution (Fig. 3a).

3.2.3. Influence of bubble size

Bubbles in boiling flow are subject to complex physical phenomena (evaporation, condensation, turbulence, coalescence, etc.) that affect their size. The bubble size varies significantly along the flow, as well as in the radial direction to the flow. Four different calculations with different models of local bubble diameter were performed (Fig. 4). The experimental values represent the local bubble Sauter diameter. In the first two calculations, constant values for bubble diameters were used (1 and 4 mm). The calculation denoted as "linear" means that the bubble diameter d_b is modelled as a linear function of local liquid subcooling, according to Eq. (21). The bubble diameters at the reference liquid subcooling temperatures of 5 and −2 K were set to the values of 1 and 3.8 mm for the conditions of the considered experiment (as in the work of Končar and

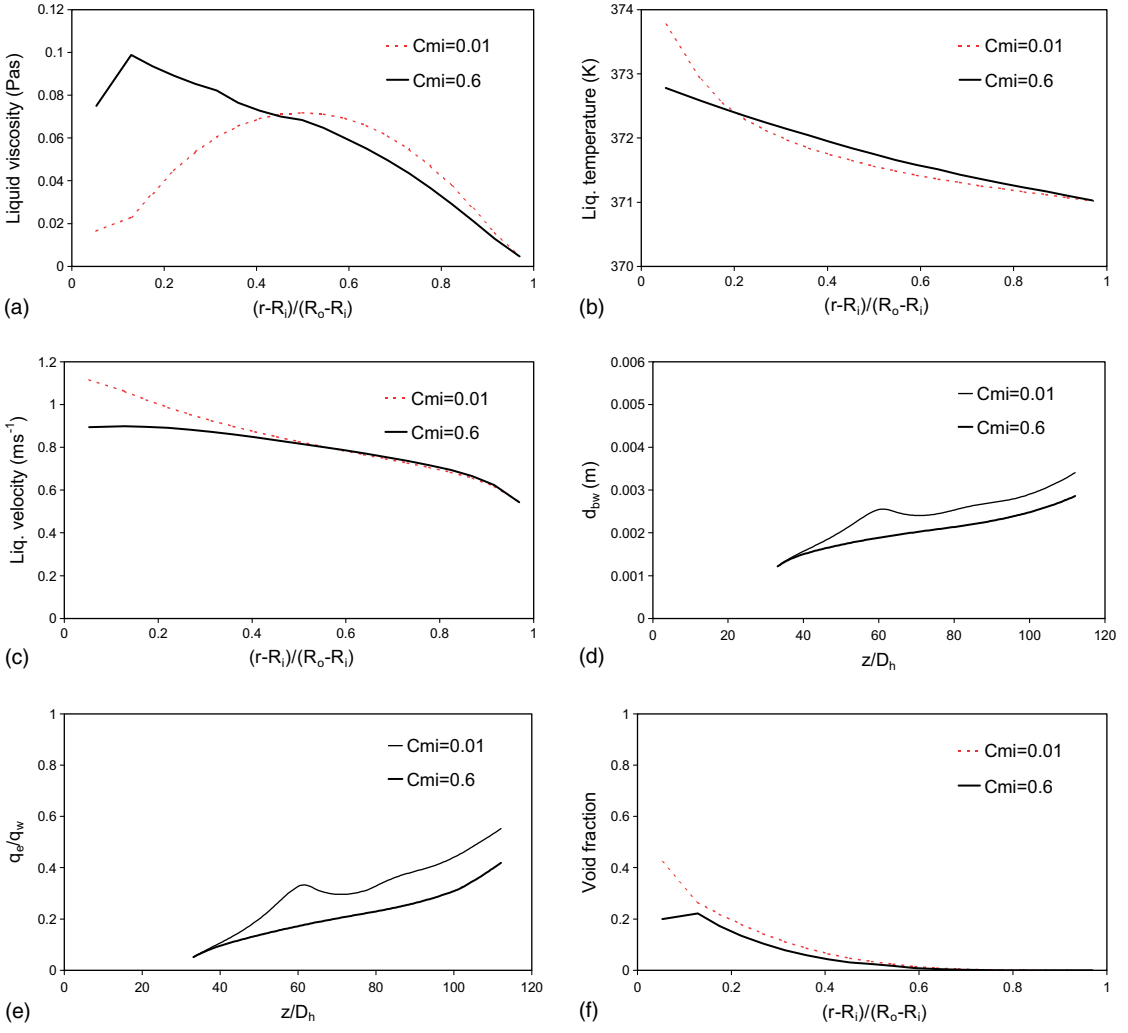

Fig. 2. Influence of bubble-induced turbulence (at axial location $z/D_h = 98.7$; [1], case 4).

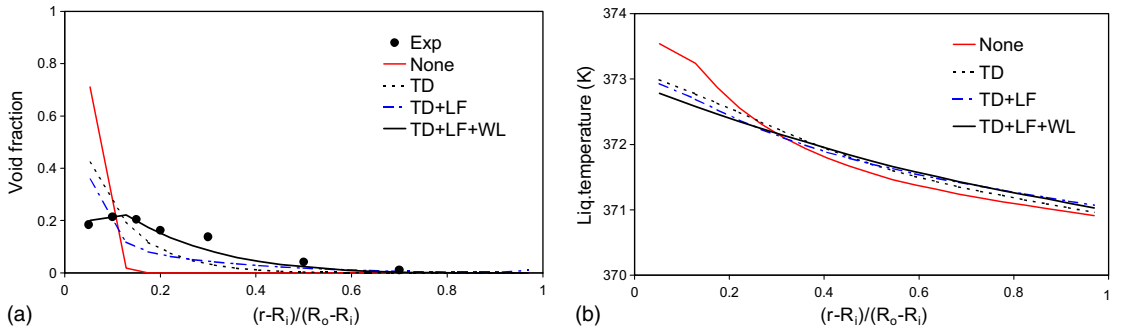

Fig. 3. Influence of non-drag forces (at axial location $z/D_h = 98.7$; [1], case 4).

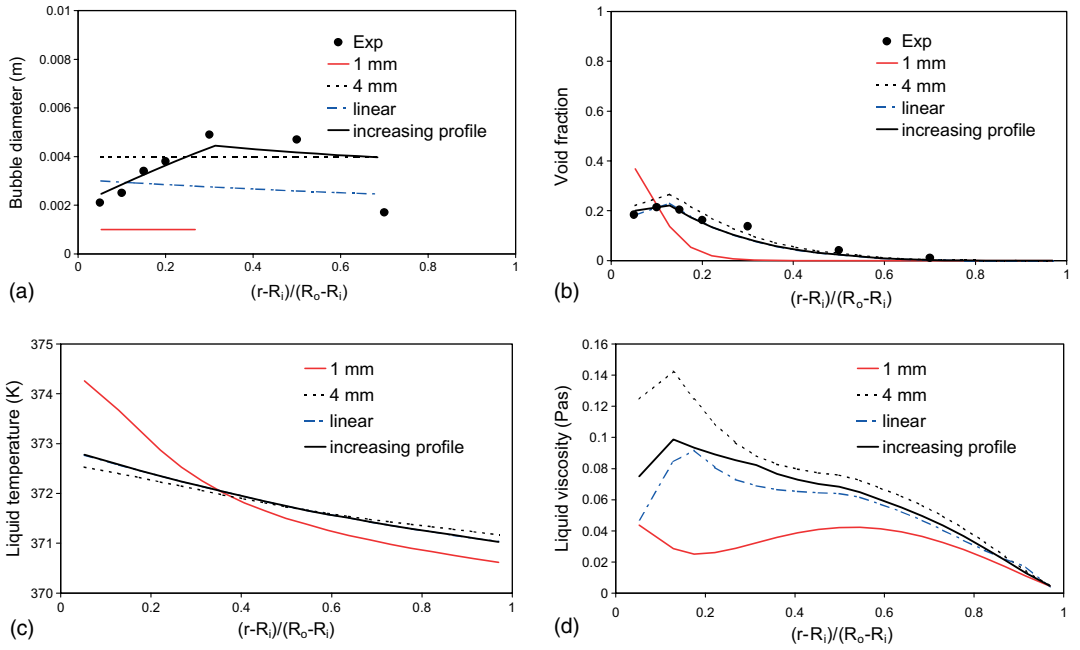

Fig. 4. Influence of bubble diameter modelling (at axial location $z/D_h = 98.7$; [1], case 4).

Mavko [37]). Outside this subcooling range, the diameters are assumed to be constant (boundary values are extrapolated). In the calculation denoted as "increasing profile", the bubble diameter is modelled according to Eq. (23) proposed in this paper. A comparison of bubble diameters in Fig. 4a shows that the "increasing profile" model exhibits a good agreement against the experimental data. Radial void fraction profiles are presented in Fig. 4b. Except in the "1 mm" calculation case, different bubble diameter modelling does not exhibit a significant influence on the radial void fraction distribution. In the case of 1 mm bubble size, the void fraction maximum is much higher and is located at the wall. Namely, due to small bubble diameter, the wall lubrication force is too weak to transport the bubbles away from the wall. A small bubble diameter also increases the condensation rate, so that the two-phase region is much narrower. Fig. 4c shows radial profiles of liquid temperature, where the highest temperature gradient at the wall can be observed in the case of 1 mm bubble diameter and the lowest in the case of 4 mm bubble diameter. As discussed previously, a high temperature gradient near the wall is a consequence of low turbulent mixing in the wall region. According to Eq. (2), the bubble-induced viscosity is directly proportional to the bubble diameter d_b. A comparison of liquid viscosities (Fig. 4d) for different bubble models confirms that the least intense turbulent mixing occurs in the case of the smallest bubble diameter.

3.3. Simulation of experimental data

As illustrative examples, Fig. 5 shows the evolution of the calculated partitioning of the wall heat flux along the heated channel for two of Bartel's experiments. In both cases, the single-phase convection heat flux gradually decreases, while quenching and evaporation heat fluxes increase. Most of the heat flux is transferred to the liquid phase. The evaporation heat flux fraction does not exceed 0.5 of the wall heat flux, even near the end of the heated length. Due to the relatively low inlet subcooling, boiling is initiated already at the beginning of the heated section in both cases. For the experimental case 4, a fully developed boiling region ($q_{1\phi} = 0$) may be observed at the end of the heated section. The transition from partially developed to the fully developed boiling region coincides with the rapid increase of average void fraction, as shown in Fig. 6.

Fig. 7 presents radial distributions of void fraction and local bubble diameter at three different axial locations for Bartel's experiments [1] (see Table 1). In general, the predicted evolution of the two-phase region along the tube agrees with the experimental observation: as boiling develops along the heated wall, the two-phase region widens, the void fraction maximum increases and shifts away from the wall. Although some discrepancies between measured and predicted results of individual radial profiles may be observed, in general, the axial evolutions of void fraction and bubble diameter profiles

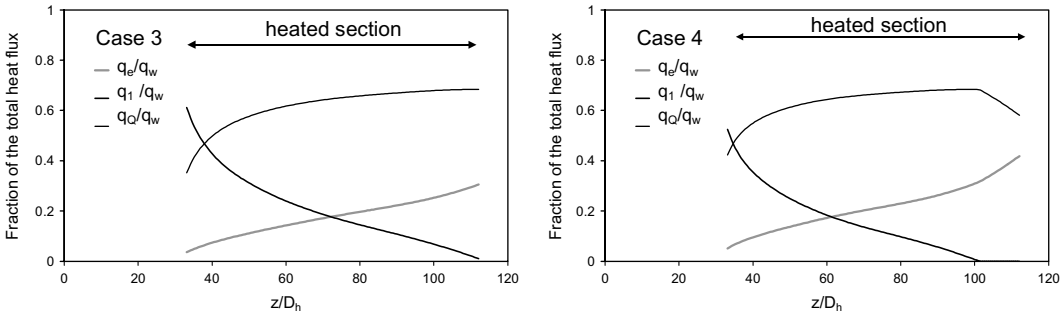

Fig. 5. Calculated heat flux partitioning along the heated channel [1].

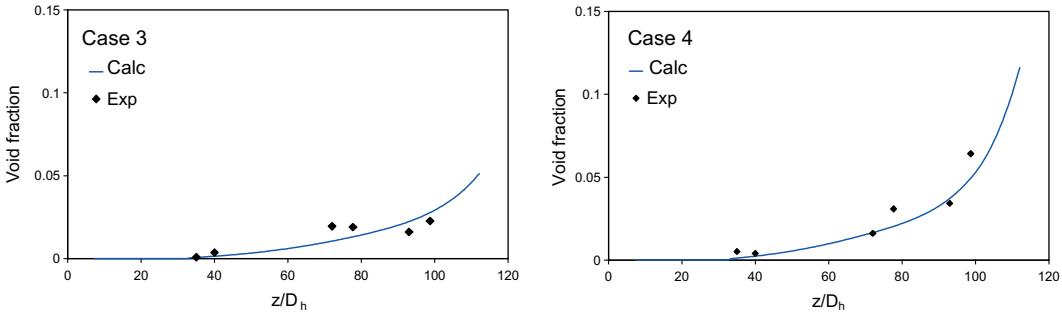

Fig. 6. Distribution of averaged void fraction along the heated channel [1].

(experimental values represent the bubble Sauter diameter) are successfully reproduced. This indicates that the proposed modelling approach captures basic mechanisms that control low-pressure subcooled boiling in vertical upward flow.

For case 1, a reasonable agreement of void fraction profiles at the lowest and the highest axial location may be observed, whereas the calculated local void fraction at the intermediate location somewhat underpredicts the experimental data. For case 2, a good agreement of void fraction at the lowest axial location, underprediction at the intermediate axial location and an extremely high discrepancy of void fraction results at the highest location can be noted. However, the measured void fraction values at the highest location are most unusual, since one would not expect the void fraction at the highest location to be lower than the void fraction at an intermediate location. Similar agreement of void fraction profiles as in case 1 can be observed in case 3 (good at the lowest and at the highest axial location and underprediction of void fraction at the intermediate location). For cases 4 and 5, the void fraction is somewhat underpredicted at the lowest and intermediate axial locations, whereas quite good agreement at the highest location may be observed.

In general, the calculated local bubble diameter profiles assume similar shapes as measured profiles. Considering the radial direction away from the wall, the increase of bubble diameter in the near-wall region is followed by a decrease of bubble diameter towards the outer adiabatic wall. The best agreement with measured bubble diameter data may be observed in cases 3, 4 and 5 with the same mass flow rate, whereas the agreement is less satisfactory in cases 1 and 2 with different mass flow rates.

It should be mentioned that the proposed two-fluid model experienced some difficulties in the cases 1 and 2. A reasonable prediction of void fraction for these two cases, presented in Fig. 7, was achieved by adjusting the coefficient C_{bw} in the correlation for bubble departure diameter d_{bw} (Eq. (20)) to the values 3 and 1.5 for the experimental cases 1 and 2, respectively. Since the local void fraction of the considered experiments is always below 0.3, bubble coalescence at the heated surface is not expected to be a major reason for these necessary adjustments of bubble departure diameter. The enhanced variation of bubble departure size may be due to sliding of bubbles in the thermal boundary layer adjacent to the heated wall. Namely, according to Prodanovic et al. [28], the sliding distance and bubble

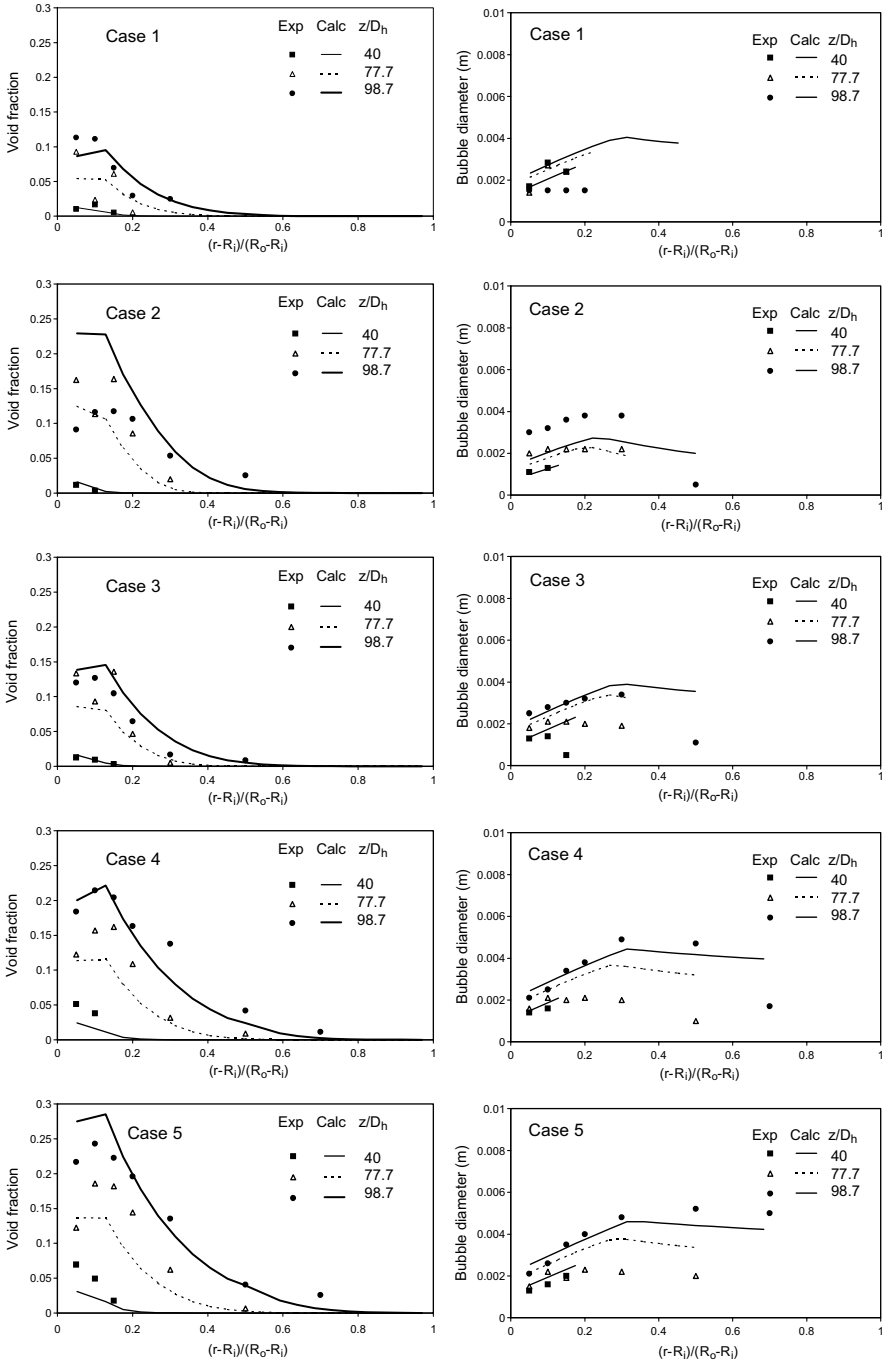

Fig. 7. Radial distributions of void fraction and local bubble diameter for Bartel's experiments [1].

departure size strongly depend on the variation of mass flow rate and heat flux in the range of low Bond numbers, $Bo < 5 \times 10^{-4}$, to which conditions for all simulated experiments in this paper belong. This underlines the need for further improvement of bubble departure size model, which should take into account a better description of bubble sliding phenomenon.

Comparisons between calculated and measured void fraction radial profiles of Lee et al. [2] experiments are presented in Fig. 8. The value of C_{bw} remained

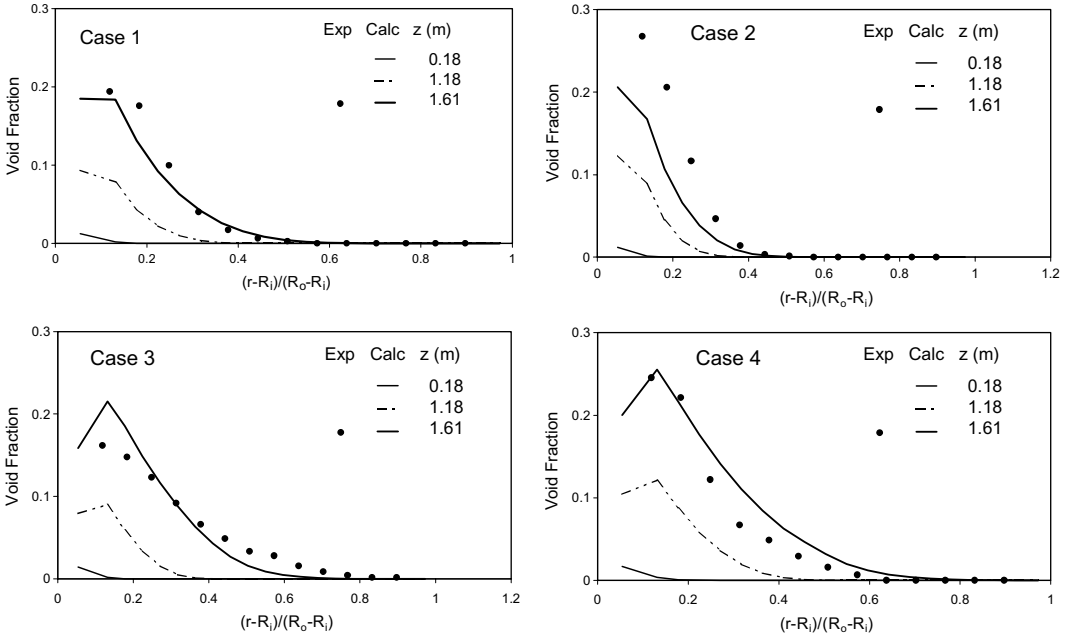

Fig. 8. Radial distributions of void fraction for Lee et al. experiments [2].

unchanged ($C_{bw} = 2$) in all calculations. Although the measurements of local void fraction were performed only at one axial location ($z = 1.61$ m), the simulation results at two other axial locations are also presented in the figures to illustrate the simulated evolution. A good agreement between predictions and experimental data may be observed for three out of four experimental cases. The local void fraction is significantly underpredicted only for the experimental case 2.

4. Conclusions

A two-fluid model of subcooled nucleate boiling flow in a vertical channel at low-pressure conditions was proposed. The model allows the simulation of the gradual evolution of the flow structure along the channel due to hydrodynamic and thermal mechanisms.

A good overall agreement between calculated and experimental data from the literature was obtained. The analysis of results also highlighted the importance of the following two phenomena in the modelling of subcooled boiling flow at low-pressure conditions:

- lateral hydrodynamic mechanisms: lift force, wall lubrication force and mixing due to bubble-induced turbulence,
- variation of bubble diameter according to local flow conditions.

Acknowledgements

The financial support of the Ministry of Education, Science and Sports of the Republic of Slovenia under Research programme P0-0505-0106 is gratefully acknowledged.

References

[1] M.D. Bartel, Experimental investigation of subcooled boiling, M.S.N.E. Thesis, Purdue University, West Lafayette, IN, USA, 1999.
[2] T.H. Lee, G.C. Park, D.J. Lee, Local flow characteristics of subcooled boiling flow of water in a vertical concentric annulus, Int. J. Multiphase Flow 28 (2002) 1351–1368.
[3] C.C. St Pierre, S.G. Bankoff, Vapor volume profiles in developing two-phase flow, Int. J. Heat Mass Transfer 10 (1967) 237–249.
[4] H. Anglart, O. Nylund, CFD application to prediction of void distribution in two-phase bubbly flows in rod bundles, Nucl. Eng. Des. 163 (1996) 81–98.
[5] K. Sekoguchi, O. Tanaka, S. Esaki, N. Katsuki, M. Nakasatomi, Prediction method of flow patterns in subcooled and low quality boiling regions, Bull. Jpn. Soc. Mech. Eng. 24 (1981) 834–841.
[6] N. Kurul, M.Z. Podowski, Multidimensional effects in forced convection subcooled boiling, in: Proceedings of the Ninth International Heat Transfer Conference, vol. 2, August 19–24, Jerusalem, Israel, 1990, pp. 21–26.

[7] J.C. Lai, B. Farouk, Numerical simulation of subcooled boiling and heat transfer in vertical ducts, Int. J. Heat Mass Transfer 36 (1993) 1541–1551.
[8] R.T. Lahey Jr., D.A. Drew, The analysis of two-phase flow and heat transfer using a multidimensional, four field, two-fluid model, Nucl. Eng. Des. 204 (2001) 29–44.
[9] R.P. Roy, S. Kang, J.A. Zarate, A. Laporta, Turbulent subcooled boiling flow—experiments and simulations, J. Heat Transfer 124 (2002) 73–93.
[10] S. Hari, Y.A. Hassan, Improvement of the subcooled boiling model for low-pressure conditions in thermal-hydraulic codes, Nucl. Eng. Des. 216 (2002) 139–152.
[11] B. Končar, B. Mavko, Modelling of low-pressure subcooled flow boiling using the RELAP5 code, Nucl. Eng. Des. 220 (2003) 255–273.
[12] G. Janssens-Maenhout, J.U. Knebel, U. Mueller, Subcooled nucleate boiling at low pressure and low heat flux, in: Proceedings of 3rd International Conference on Multiphase Flow, June 8–12, Lyon, France, 1998.
[13] J.Y. Tu, G.H. Yeoh, On numerical modelling of low pressure subcooled boiling flows, Int. J. Heat Mass Transfer 45 (2002) 1197–1209.
[14] D. Juric, G. Tryggvason, Computation of boiling flows, Int. J. Multiphase Flow 24 (1998) 387–410.
[15] D. Legendre, J. Boree, J. Magnaudet, Thermal and dynamic evolution of a spherical bubble moving steadily in a superheated or subcooled liquid, Phys. Fluids 10 (1998) 1256–1272.
[16] G.A. Mortensen, J.A. Trapp, Two-phase flow modeling with discrete particles, in: Proceedings of the ASME Heat Transfer Division, Two-Phase Flow in Energy Exchange Systems, vol. 220, pp. 73–85, 1992.
[17] I. Kljenak, G.C. Park, B. Mavko, T. Lee, Bubble-tracking modeling of subcooled nucleate boiling in a vertical annulus, in: Proceedings of the Twelfth International Heat Transfer Conference, August 18–23, Grenoble, France, 2002, pp. 767–772.
[18] M. Ishii, Thermo-fluid dynamic theory of two-phase flow, Eyrolles, Paris, 1975.
[19] M. Leskovar, B. Mavko, An original combined multiphase model of the steam-explosion premixing phase, J. Mech. Eng. 48 (2002) 438–448.
[20] CFX-4.3 Solver Manual, AEA Technology plc, Harwell, United Kingdom, 1999.
[21] Y. Sato, M. Sadatomi, K. Sekoguchi, Momentum and heat transfer in two-phase bubble flow—I. Theory, Int. J. Multiphase Flow 7 (1981) 167–177.
[22] B.E. Launder, D.B. Spalding, Mathematical Models of Turbulence, Academic Press, New York, 1972.
[23] M. Ishii, N. Zuber, Drag coefficient and relative velocity in bubbly, droplet or particulate flows, AIChE J. 25 (1979) 843–855.
[24] R.T. Lahey Jr., The CFD analysis of multidimensional phenomena in multiphase flow, in: Proceedings of 2nd International Conference on Multiphase Flow, April 3–7, Kyoto, Japan, 1995.
[25] S.P. Antal, R.T. Lahey Jr., J.E. Flaherty, Analysis of phase distribution in fully developed laminar bubbly two-phase flow, Int. J. Multiphase Flow 17 (1991) 635–652.
[26] E.L. Bibeau, M. Salcudean, Subcooled void growth mechanisms and prediction at low pressure and low velocity, Int. J. Multiphase Flow 20 (1994) 837–863.
[27] O. Zeitoun, M. Shoukri, Bubble behavior and mean diameter in subcooled flow boiling, J. Heat Transfer 118 (1996) 110–116.
[28] V. Prodanovic, D. Fraser, M. Salcudean, Bubble behavior in subcooled flow boiling of water at low pressures and low flow rates, Int. J. Multiphase Flow 28 (2002) 1–19.
[29] G. Meister, Vapour bubble growth and recondensation in subcooled boiling flow, Nucl. Eng. Des. 54 (1979) 97–114.
[30] H. Victor, M. Del Valle, D.B.R. Kenning, Subcooled flow boiling at high heat flux, Int. J. Heat Mass Transfer 28 (1985) 1907–1920.
[31] N. Kurul, Multidimensional effects in two-phase flow including phase change, Ph.D. Thesis, Rensselaer Polytechnic Institute, Troy, NY, USA, 1990.
[32] H.J. Ivey, Relationships between bubble frequency, departure diameter and rise velocity in nucleate boiling, Int. J. Heat Mass Transfer 10 (1967) 1023–1040.
[33] M. Lemmert, J.M. Chawla, Influence of flow velocity on surface boiling heat transfer coefficient, in: E. Hahne, U. Grigull (Eds.), Heat Transfer in Boiling, Academic Press and Hemisphere, 1977.
[34] H.C. Unal, Maximum bubble diameter, maximum bubble-growth time and bubble-growth rate, Int. J. Heat Mass Transfer 19 (1976) 643–649.
[35] V. Chatoorgoon, G.R. Dimmick, M.B. Carver, W.N. Selander, Application of generation and condensation models to predict subcooled boiling void at low pressures, Nucl. Technol. 98 (1992) 366–378.
[36] B. Končar, Model of forced convective subcooled boiling at low pressure conditions, Ph.D. Thesis, Faculty of Mathematics and Physics, University of Ljubljana, Slovenia, 2002.
[37] B. Končar, B. Mavko, CFD simulation of subcooled flow boiling at low pressure, in: Proceedings of International Conference Nuclear Energy in Central Europe, September 10–13, Portorož, Slovenia, 2001.